Rate Models for Conductance-Based Cortical Neuronal Networks

Oren Shriki
orens@fiz.huji.ac.il
Racah Institute of Physics, Hebrew University, Jerusalem 91904, Israel, and
Center for Neural Computation, Hebrew University, Jerusalem 91904, Israel

David Hansel
david.hansel@biomedicale.univ-paris5.fr
Laboratoire de Neurophysique et Physiologie du Système Moteur,
Université René Descartes, 75270 Paris cedex 06, Paris, France, and
Center for Neural Computation, Hebrew University, Jerusalem 91904, Israel

Haim Sompolinsky
haim@fiz.huji.ac.il
Racah Institute of Physics, Hebrew University, Jerusalem 91904, Israel, and
Center for Neural Computation, Hebrew University, Jerusalem 91904, Israel

Population rate models provide powerful tools for investigating the principles that underlie the cooperative function of large neuronal systems. However, biophysical interpretations of these models have been ambiguous. Hence, their applicability to real neuronal systems and their experimental validation have been severely limited. In this work, we show that conductance-based models of large cortical neuronal networks can be described by simplified rate models, provided that the network state does not possess a high degree of synchrony. We first derive a precise mapping between the parameters of the rate equations and those of the conductance-based network models for time-independent inputs. This mapping is based on the assumption that the effect of increasing the cell's input conductance on its f-I curve is mainly subtractive. This assumption is confirmed by a single compartment Hodgkin-Huxley type model with a transient potassium A-current. This approach is applied to the study of a network model of a hypercolumn in primary visual cortex. We also explore extensions of the rate model to the dynamic domain by studying the firing-rate response of our conductance-based neuron to time-dependent noisy inputs. We show that the dynamics of this response can be approximated by a time-dependent second-order differential equation. This phenomenological single-cell rate model is used to calculate the response of a conductance-based network to time-dependent inputs.

1 Introduction

Theoretical models of the collective behavior of large neuronal systems can be divided into two categories. One category attempts to incorporate the known microscopic anatomy and physiology of the system. To study these models, numerical simulations are required. They involve a large number of parameters whose precise values are unknown, and the systematic exploration of the model parameter space is impractical. Furthermore, due to their complexity, it is hard to construct a qualitative interpretation of their behavior. The second category consists of simplified models that retain only some gross features of the modeled system, thereby allowing for systematic analytical and numerical investigations. These models have been extremely useful in extracting qualitative principles underlying such functions as memory, visual processing, and motor control (Amit, 1989; Churchland & Sejnowski, 1992; Georgopoulos & Lukashin, 1993; Ben-Yishai, Lev Bar-Or, & Sompolinsky, 1995; Seung, 1996; Zhang, 1996; Salinas & Abbott, 1996; Hansel & Sompolinsky, 1998; Rolls & Treves, 1998).

Simplified models of large neuronal systems are often cast in the form of rate models, in which the state of the network units is characterized by smooth rate variables (Wilson & Cowan, 1972; Hopfield, 1984). These variables are related to the units' synaptic inputs via a nonlinear input-output transfer function. The input is a linear sum of the presynaptic activities, whose coefficients are termed the *synaptic weights* of the network. Unfortunately, the use of rate models for concrete neuronal systems has been limited by the lack of a clear biophysical interpretation of the parameters appearing in these models. In particular, the relation between activity variables, input variables, and synaptic weights, on one hand, and physiologically measured quantities, on the other, is obscure. Furthermore, quite often rate models predict that the network should settle in a fixed point where the network activities, as well as synaptic inputs, are time independent. However, the biological meaning of this fixed-point state is unclear, since neither the postsynaptic currents nor the postsynaptic potentials are constant in time if the cells are active. It is thus important to inquire whether there is a systematic relation between real neuronal systems and simple rate models.

Several studies have derived reduced-rate models for networks of spiking neurons (Amit & Tsodyks, 1991; Abbott & Kepler, 1990; Ermentrout, 1994). In particular, it has been shown that if the synaptic time constants are long, the network dynamics can be reduced to rate equations that describe the slow dynamics of the synaptic activities (Ermentrout, 1994). However, the assumption of slow synaptic dynamics is inadequate for modeling cortical networks, where fast synapses play a dominant role. Here, we show that asynchronous states of large cortical networks described by conductance-based dynamics can be described in terms of simple rate equations, even when the synaptic time constants are small. A simple mapping between the synaptic conductances and the synaptic weights is derived. We apply our

method to study the properties of conductance-based networks that model a hypercolumn in visual cortex. The simple reduction of conductance-based networks to rate models is restricted to asynchronous states that exist only if the networks are driven by stationary inputs. We derive a more complex rate model, which is appropriate to describe the synchronous response of large conductance-based networks to weakly nonstationary noisy synaptic inputs. Our results provide a framework for using rate models to quantitatively predict the extracellular and intracellular response properties of large cortical networks.

2 Models and Methods

2.1 Dynamics of a Single-Compartment Cell. Our starting point is the dynamic equation of a single-compartment neuron,

$$C\frac{dV(t)}{dt} = g_L(E_L - V(t)) - I^{active}(t) + I^{app}(t), \tag{2.1}$$

where $V(t)$ is the membrane potential of the cell at time t, C is its capacitance, g_L is the leak conductance, and E_L is the reversal potential of the leak current. Besides the leak current, the cell has active ionic currents with Hodgkin-Huxley type kinetics (Hodgkin & Huxley, 1952), the total sum of which is denoted as $I^{active}(t)$ in equation 2.1. An externally injected current is denoted as I^{app}. If I^{app} is constant in time and is sufficiently large, the cell will fire in a repetitive manner with a steady-state firing rate f. In general, the relation between the applied current, I, and the firing rate, f, defines a function $f = F(I, g_L)$, called the *f-I curve*. The second argument, g_L, expresses the dependence of the input-output function of the neuron on the magnitude of the leak conductance. This dependence is an important factor in our work, as will become clear. The form of the function F depends on the active currents comprising I^{active}. In many cortical neurons, the f-I curve is approximately linear for I above threshold (Azouz, Gray, Nowak, & McCormick, 1997; Ahmed, Anderson, Douglas, Martin, & Whitteridge, 1998; Stafstrom, Schwindt, & Crill, 1984) and can be captured by the following equation,

$$f = \beta[I - I_c]_+, \tag{2.2}$$

where $[x]_+ \equiv x$ for $x > 0$ and is zero otherwise; β is the gain parameter. This behavior can be modeled by a Hodgkin-Huxley type single compartment neuron with a slow A-current (Hille, 1984). (See appendix A for the details of the model.) The parameters of the sodium and the potassium currents were chosen to yield a saddle-node bifurcation at the onset of firing. Figure 1 shows the response of this model neuron without and with the A-current. As can be seen, the A-current linearizes the f-I relationship. Our model neuron has gain value $\beta = 35.4$ cm$^2/\mu$Asec.
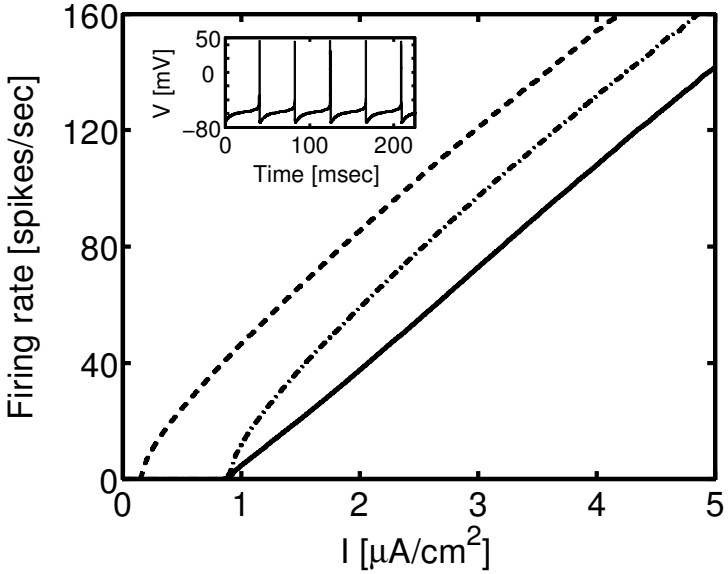
Figure 1: f-I curves of the single-neuron model with $g_A = 0$ (dashed line), $g_A = 20\,\text{mS/cm}^2$, $\tau_A = 0\,\text{msec}$ (dash-dotted line), $g_A = 20\,\text{mS/cm}^2$, $\tau_A = 20\,\text{msec}$ (solid line). Comparison of the three curves shows that linearization of the f-I curve is due to the long time constant of the A-current. (Inset) A voltage trace of the single-neuron model with constant current injection of amplitude $I = 1.6\ \mu\text{A/cm}^2$ for $g_A = 20\,\text{mS/cm}^2$, $\tau_A = 20\,\text{msec}$. The neuron's parameter values are as defined in appendix A.

Relatively few experimental data have been published on the dependence of the firing rate of cortical cells on their leak conductance. However, experimental evidence (Connors, Malenka, & Silva, 1988; Brizzi, Hansel, Meunier, van Vreeswijk, & Zytnicki, 2001) and biophysical models (Kernell, 1968; Holt & Koch, 1997) show that increasing g_L affects the f-I curve primarily by increasing its threshold current, whereas its effect on the gain of the curve is weak. We incorporate these properties by assuming that β is independent of g_L and that the threshold current increases linearly with the leak conductance,

$$I_c = I_c^o + V_c g_L. \tag{2.3}$$

The *threshold gain potential* V_c measures the rate of increase of the threshold current as the leak conductance, g_L, increases, and I_c^o is the threshold current when $g_L = 0$. This behavior is also reproduced in our model neuron, as shown in Figure 2. Approximating the f-I curve with equations 2.2 and 2.3 yields $I_c^o = 0.63\ \text{mA/cm}^2$ and $V_c = 5.5\ \text{mV}$. This provides a good
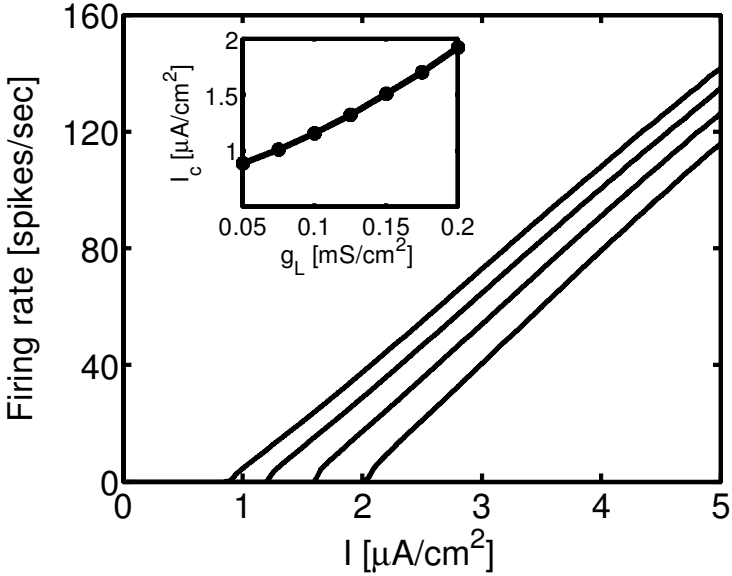
Figure 2: f-I curves for $g_A = 20$ mS/cm^2, $\tau_A = 20$ msec, and different values of g_L. The curves from left to right correspond to $g_L = 0.05, 0.1, 0.15, 0.2$ mS/cm^2, respectively. (Inset) The threshold current, I_c, as a function of the leak conductance, g_L.

approximation of the f-I curve for the range $f = 5$–150 spikes/sec. For higher firing rates, the effect of the saturation of the rates becomes significant and needs to be incorporated into the model. We have found that this effect can be described approximately by an f-I curve of the form

$$f = \beta[I - I_c]_+ - \gamma[I - I_c]_+^2, \tag{2.4}$$

with I_c given by equation 2.3. Fitting the firing rate of our single-neuron model to equation 2.4 yields good fit over the range $f = 5$–300 spikes/sec, with the parameter values $\beta = 39.6$ cm^2/μAsec, $\gamma = 0.86$ (cm^2/μA)^2/sec, $\alpha = 6.77$ mV, and $I_c^o = 0.59$ μA/cm^2. The above conductance-based model neuron is the one used in all subsequent numerical analyses.

2.2 Network Dynamics. The network dynamics of N coupled cells are given by

$$C\frac{dV_i}{dt} = g_L(E_L - V_i(t)) - I_i^{active} + I_i^{ext} + I_i^{net} \quad (i = 1, \ldots, N), \tag{2.5}$$

where I_i^{net} denotes the synaptic current of the postsynaptic cell i generated by the presynaptic sources within the network. It is modeled as

$$I_i^{net}(t) = \sum_{j=1}^{N} g_{ij}(t)(E_j - V_i(t)), \tag{2.6}$$

where $g_{ij}(t)$ is the synaptic conductance triggered by the action potentials of the presynaptic jth cell and E_j is the reversal potential of the synapse. The synaptic conductance is assumed to consist of a linear sum of contributions from each of the presynaptic action potentials. In our simulations, $g_{ij}(t)$ has the form of an instantaneous jump from 0 to G_{ij} followed by an exponential decay with a synaptic decay time τ_{ij},

$$\frac{dg_{ij}}{dt} = -\frac{g_{ij}}{\tau_{ij}} + G_{ij}R_j(t), \quad t > 0, \tag{2.7}$$

where $R_j(t) = \sum_{t_j} \delta(t - t_j)$ is the instantaneous firing rate of the presynaptic jth neuron and t_j are the times of occurrence of its spikes. In general, we define G_{ij} as the peak of $g_{ij}(t)$ and the synaptic time constant as $\tau_{ij} = \int_0^\infty g_{ij}(t)\,dt/G_{ij}$.

Synaptic currents from presynaptic sources outside the network are denoted by I_i^{ext}. For simplicity, we assume that these sources are all excitatory with the same reversal potential, E^{inp}, peak conductance G^{inp}, and synaptic time constant, τ^{inp}. We assume that these sources fire Poisson trains of action potentials asynchronously, which generate synaptic conductances with dynamics similar to equation 2.7. Under these assumptions, their summed effects on the postsynaptic neuron i can be represented by a single effective excitatory synapse with peak conductance, G^{inp}, time constant τ^{inp}, and activated by a single Poisson train of spikes with average rate f_i^{inp} which is the summed rate of all the external sources to the ith neuron. Thus, the external current on neuron i can be written as

$$I_i^{ext}(t) = g_i^{inp}(t)(E^{inp} - V_i(t)). \tag{2.8}$$

The quantity $g_i^{inp}(t)$ satisfies an equation similar to equation 2.7,

$$\frac{dg_i^{inp}}{dt} = -\frac{g_i^{inp}}{\tau^{inp}} + G^{inp}R_i^{inp}(t), \quad t > 0, \tag{2.9}$$

where R_i^{inp} is a Poisson spike train with mean rate f_i^{inp}. The value of f_i^{inp} is specified below for each of the concrete models that we study. Due to the Poisson statistics of R_i^{inp}, the external conductance, $g_i^{inp}(t)$, is a random variable with a time average and variance $G^{inp}f_i^{inp}\tau^{inp}$ and $(G^{inp})^2 f_i^{inp}\tau^{inp}/2$,

respectively. Note that $f_i^{\text{inp}} \tau^{\text{inp}}$ is the mean number of input spikes arriving within a single synaptic integration time. The fluctuations in R_i^{inp} constitute the noise in the external input to the network. We define the coefficient of variation of this noise as the ratio of its standard deviation and its mean, that is, $\Delta_i = 1/\sqrt{2 f_i^{\text{inp}} \tau^{\text{inp}}}$. As expected, the coefficient of variation is proportional to the inverse square root of the total number of spikes arriving within a single synaptic integration time. In particular, one can increase the noise level of the input by decreasing f_i^{inp} and increasing G^{inp} while keeping their product constant.

Time-dependent inputs are modeled by a Poisson process with a rate that is modulated in time. In most of the examples studied in this article, we assume a sinusoidal modulation—that the instantaneous firing rate in the external input to the neuron is

$$f^{\text{inp}}(t) = f_0^{\text{inp}} + f_1^{\text{inp}} \cos(\omega t), \tag{2.10}$$

where $\omega/2\pi$ is the frequency of the modulation.

2.3 Model of a Hypercolumn in Primary Visual Cortex. We model a hypercolumn in visual cortex by a network consisting of N_e excitatory neurons and N_{in} inhibitory neurons that are selective to the orientation of the visual stimulus in their common receptive field. We impose a ring architecture on the network. The cortical neurons are parameterized by an angle θ, which denotes their preferred orientation (PO). The ith excitatory neuron is parameterized by $\theta_i = -\frac{\pi}{2} + i\frac{\pi}{N_e}$, and similarly for the inhibitory ones. The peak conductances of the cortical recurrent excitatory and inhibitory synapses decay exponentially with the distance between the interacting neurons, measured by the dissimilarity in their preferred orientations, that is,

$$G_\alpha(\theta - \theta') = \frac{\bar{G}_\alpha}{\lambda_\alpha} \exp(-|\theta - \theta'|/\lambda_\alpha), \tag{2.11}$$

where $\theta - \theta'$ is the difference between the POs of the pre- and postsynaptic neurons. The index α takes the values e and in. The quantity G_e (resp. G_{in}) denotes an excitatory (inhibitory) interaction (targeting either excitatory or inhibitory neurons) with a space constant λ_e (resp. λ_{in}). Note that the excitatory as well as the inhibitory interactions are the same for excitatory and inhibitory targets. Additional excitatory neurons provide external input to the network, representing the lateral geniculate nucleus (LGN) input to cortex, each with peak conductance $G^{\text{inp}} = \bar{G}_{LGN}$. The total mean firing rate of the afferent inputs to a neuron with PO θ is $f^{\text{inp}} = f_{LGN}(\theta - \theta_0)$, where

$$f_{LGN}(\theta - \theta_0) = \bar{f}_{LGN} C[(1 - \epsilon) + \epsilon \cos(2(\theta - \theta_0))]. \tag{2.12}$$

The parameter C is the stimulus contrast, and the angle θ_0 denotes the orientation of the stimulus. The parameter ϵ measures the degree of tuning of the LGN input. If $\epsilon = 0$, the LGN input is untuned: all the neurons receive the same input from the LGN, regardless of their PO and the orientation of the stimulus. If $\epsilon = 0.5$, the LGN input vanishes for neurons with a PO that is orthogonal to the stimulus orientation. The maximal LGN rate $\bar{f}_{LGN}$ is the total firing rate of the afferents of a stimulus with $C = 1$ and $\theta = \theta_0$. The single-neuron dynamics is given by equation 2.1 and is assumed to be the same for both the excitatory and inhibitory populations.

2.4 Numerical Integration and Analysis of Spike Responses. In the numerical simulations of the conductance-based networks, the nonlinear differential equations of the neuronal dynamics were integrated using a fourth-order Runge-Kutta method (Press, Flannery, Teukolsky, & Vetterling, 1988) with a fixed time step Δt. Most of the simulations were performed with $\Delta t = 0.05$ msec. In order to check the stability and precision of the results, some simulations were also performed with $\Delta t = 0.025$ msec.

A spike event is counted each time the voltage of a neuron crosses a fixed threshold value $V_{th} = 0$. We measure the instantaneous firing rate of a single neuron defined as the number of spikes in time bins of size $\Delta t = 0.05$ msec, averaged over different realizations of the external input noise. We then compute the time average of this response and, in the case of periodically modulated input, the amplitude and phase of its principal temporal harmonic. We also measure the population firing rate, defined as the number of spikes of single neurons in each time bin divided by Δt, averaged over a select population of neurons in the network as well as over the input noise. As in the case of a single neuron, the network response is characterized by the time average and the principal harmonic of the population rate.

3 Rate Equations for General Asynchronous Neuronal Networks

The dynamic states of a large network characterized by the above equations can be classified as being synchronous or asynchronous (Ginzburg & Sompolinsky, 1994; Hansel & Sompolinsky, 1996), which differ in terms of the strength of the correlation between the temporal firing of different neurons. When the external currents, I_i^{ext}, are constant in time (except for a possible noisy component which is spatially uncorrelated), the network may exhibit an asynchronous state in which the activities of the neurons are only weakly correlated. Formally, in an asynchronous state, the correlation coefficients between the voltages of most of the neuronal pairs approach zero in the limit where the network size, N, grows to infinity.

Analyzing the asynchronous state in a highly connected network is relatively simple. Because each postsynaptic cell is affected by many uncorrelated synaptic conductances (within a window of its integration time), these

conductances can be taken to be time independent. In other words, in the asynchronous state, the spatial summation of the synaptic conductances is equivalent to a time average. Hence, the total synaptic current of each cell can be written as

$$I_i^{net}(t) + I_i^{ext}(t) = \sum_{j=1}^{N} G_{ij}\tau_{ij}f_j(E_j - V_i(t)) + G^{inp}\tau^{inp}f_i^{inp}(E^{inp} - V_i(t)) \quad (3.1)$$

(see equations 2.6 and 2.8). This current can be decomposed into two components:

$$I_i^{net} + I_i^{ext} = I_i^{app} + \Delta I_i^L. \tag{3.2}$$

I_i^{app} is the component of the synaptic current that has the form of a constant applied voltage-independent current

$$I_i^{app} = \sum_{j=1}^{N} G_{ij}\tau_{ij}f_j(E_j - E_L) + G^{inp}\tau^{inp}f_i^{inp}(E^{inp} - E_L). \tag{3.3}$$

The second component of the synaptic current, ΔI_i^L, embodies the voltage dependence of the synaptic current and has the form of a leak current,

$$\Delta I_i^L = g_i^{syn}(E_L - V_i(t)), \tag{3.4}$$

where

$$g_i^{syn} = g_i^{net} + g_i^{inp} \tag{3.5}$$

is the mean total synaptic conductance of the ith cell. The quantities g_i^{net} and g_i^{inp} are given by

$$g_i^{net} = \sum_{j=1}^{N} G_{ij}\tau_{ij}f_j, \tag{3.6}$$

$$g_i^{inp} = G^{inp}\tau^{inp}f_i^{inp}. \tag{3.7}$$

Thus, the discharge of the postsynaptic cell in the asynchronous network can be described by the f-I curve of a single cell with an applied current, equation 3.3, and a "leak" conductance, which is equal to $g_L + g_i^{syn}$, equation 3.5. Incorporating these contributions in equation 2.2, taking into account the dependence of the threshold current on the total passive conductance as

given by equation 2.3, yields the following equations for the firing rates of
the cells:

$$f_i = \beta[I_i^{app} - V_c(g_L + g_i^{syn}) - I_c^o]_+ \tag{3.8}$$

$$= \beta\left[\sum_{i=1}^{N} J_{ij}f_j + J^{inp}f_i^{inp} - T\right]_+, \quad (i = 1, \ldots, N),$$

where

$$J_{ij} = G_{ij}\tau_{ij}(E_j - E_L - V_c) \tag{3.9}$$

and

$$J^{inp} = G^{inp}\tau^{inp}(E^{inp} - E_L - V_c). \tag{3.10}$$

The parameter T is the threshold current of the isolated cells, $T = I_c(g_L)$.
Note that the subtractive term V_c in equations 3.9 and 3.10 is the result of the
increase of the current threshold of the cell due to the synaptic conductance
(see equation 2.3).

Equation 3.8 is of the form of the self-consistent rate equations that de-
scribe the input-output relations for the neurons in a recurrent network
at a fixed-point state. This theory provides a precise mapping between the
biophysical parameters of the neurons and synapses and the parameters ap-
pearing in the fixed-point rate equations. The output state variables, given
by the right-hand side of equation 3.8, are simply the stationary firing rates of
the neurons. The input variables, $\sum_{i=1}^{N} J_{ij}f_j + J^{inp}f_i^{inp}$, are the mean synaptic
currents at a fixed potential given by $E_L + V_c$, where V_c is the threshold-gain
potential, equation 2.3.

Equation 3.9 provides a precise interpretation of the synaptic efficacies J_{ij}
in terms of the biophysical parameters of the cells and the synaptic conduc-
tances. We note in particular that our theory yields a precise criterion for the
sign of the efficacy of the synaptic connection. According to equation 3.9,
synapses with positive efficacy obey the inequality

$$E_j > E_L + V_c. \tag{3.11}$$

Conversely, synapses with negative efficacies obey $E_j < E_L + V_c$. The po-
tential $E_L + V_c$ is close but not identical to the threshold potential of the
cell. Hence, this criterion, which takes into account the dynamics of firing
rates in the network, does not match exactly the biophysical definition of
excitatory and inhibitory synapses.

The above results allow the prediction not only of the stationary rates of
the neurons but also their mean synaptic conductances due to the input from

within the network and to the external input. In fact, using equations 3.6 and 3.7 and equations 3.9 and 3.10 yields

$$g_i^{net} = \sum_{j=1}^{N} J_{ij} \frac{f_j}{E_j - E_L - V_c} \tag{3.12}$$

and

$$g_i^{inp} = J^{inp} \frac{f_i^{inp}}{E^{inp} - E_L - V_c}. \tag{3.13}$$

In the following sections, we apply this theory to concrete network architectures.

4 Response of an Excitatory Population to a Time-Independent Input ▬

We first test the mapping equations, equations 3.8 through 3.10, in the case of a large, homogeneous network that contains N identical excitatory neurons. The network dynamics are given by equations 2.5 through 2.7 with the single-neuron model of appendix A. Each neuron is connected to all other neurons with a peak synaptic conductance, G, which is the same for all the connections in the network. In addition, each neuron receives a single external synaptic input that has a peak conductance, G^{inp}, which is activated by a Poisson process with a fixed uniform rate, f^{inp}. The external synaptic inputs to different cells are uncorrelated. The dynamic response of all synaptic conductances is given by equation 2.7 with a single synaptic time constant $\tau_e = 5$ msec.

Applying equations 3.8 through 3.10 to this simple architecture results in the following equation for the mean firing rate of the neurons in the network, f,

$$f = \beta[J^{inp} f^{inp} + Jf - I_c]_+ \tag{4.1}$$

where

$$J^{inp} = G^{inp} \tau_e (E_e - E_L - V_c) \tag{4.2}$$
$$J = N G \tau_e (E_e - E_L - V_c).$$

The solution for the firing rate is

$$f = \frac{\beta}{1 - \beta J} [J^{inp} f^{inp} - I_c]_+. \tag{4.3}$$

The mean firing rate, f, of the neurons in the network, as predicted from this equation, is displayed in Figure 3 (dashed line) against the value of the
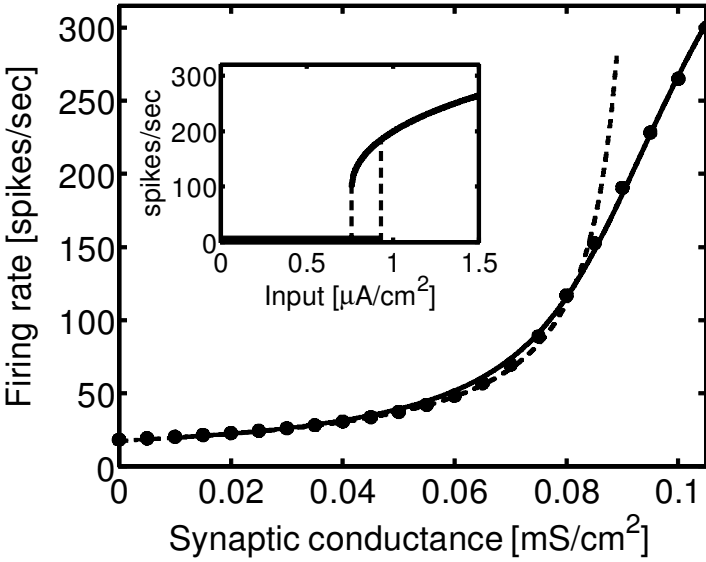
Figure 3: Firing rate versus excitatory synaptic strength in a large network of fully connected excitatory neurons. The rate of the external input is $f^{inp} = 1570$ spikes/sec, and the synaptic time constant is $\tau_e = 5$ msec. Dashed line: Analytical results from equation 4.3. Solid line: Analytical results when a quadratic fit is used for the f-I curve, equation 2.4. Circles: Results from simulations of the conductance-based model with $N = 1000$. (Inset) Firing rate versus external input for strong excitatory feedback (analytical results) showing bistability for $NG = 0.49$ μS/cm^2. The network can be either quiescent or in a stable sustained active state in a range of external inputs, $J^{inp} f^{inp}$, less than the threshold current, I_c.

peak conductance of the total excitatory feedback, NG. When the synaptic conductance increases, such that J reaches the critical value $J = 1/\beta$ (corresponding to $NG = 0.095$ mS/cm^2), the firing rate, f, diverges. However, it is expected that when the firing rate reaches high values, the weak nonlinearity of the f-I curve, given by the quadratic correction, equation 2.4, will need to be taken into account. Indeed, solving the self-consistent equation for f with the quadratic term (solid line in Figure 3) yields finite values for f, even when J is larger than $1/\beta$. In addition, the quadratic nonlinearity predicts that in the high J regime, the network should develop bistability. For a range of subthreshold external inputs, the network can be in either a stable quiescent state or a stable active state with high firing rates, as shown in the inset of Figure 3. These predictions are in full quantitative agreement with the numerical simulations of the conductance-based excitatory network as shown in Figure 3.

5 A Model of a Hypercolumn in Primary Visual Cortex

In this section we show how the correspondence between conductance-based models and rate models can be applied to investigate a model of a hypercolumn in V1.

When applying the general rate equations, equations 3.8 through 3.10, to the hypercolumn model, we first note that in the asynchronous state, the firing-rate profile of the excitatory and the inhibitory populations is the same. This is because we assume that the interaction profiles depend solely on the identity (excitatory or inhibitory) of the presynaptic neurons and that the single-neuron properties of the two types of cells are the same. We denote the rate of the (e or in) neurons with PO θ and a stimulus orientation θ_0 as $f(\theta - \theta_0)$. These rates obey

$$f(\theta - \theta_0) = \beta \left[\int_{-\pi/2}^{+\pi/2} \frac{d\theta'}{\pi} J(\theta - \theta') f(\theta' - \theta) \right.$$
$$\left. + J_{LGN} f_{LGN}(\theta - \theta_0) - T \right]_+ , \tag{5.1}$$

where we replaced the sum over the synaptic recurrent inputs by an integration over the variable θ', which is a valid approximation for a large network. The recurrent interaction profile, $J(\theta)$, combines the effect of the excitatory and the inhibitory cortical inputs and has the form

$$J(\theta - \theta_0) = \sum_{\alpha=e,in} \frac{J_\alpha}{\lambda_\alpha} \exp(-|\theta - \theta'|/\lambda_\alpha), \tag{5.2}$$

where $J_\alpha = N_\alpha \bar{G}_\alpha \tau_\alpha (E_\alpha - E_L - V_c)$, $\alpha = e, in$, and $J_{LGN} = \bar{G}_{LGN} \tau_e (E_e - E_L - V_c)$; τ_α denotes the excitatory and inhibitory synaptic time constants, and N_e, N_{in} are the number of neurons in the excitatory and inhibitory populations, respectively. Equations 5.1 and 5.2 correspond to the rate equations 3.8 through 3.10 with the synaptic conductances and input firing rate, which are given by equations 2.11 and 2.12. In appendix B, we outline the analytical solution of equations 5.1 and 5.2, which allows us to compute the neuronal activity and the synaptic conductances as functions of the model parameters.

We used the analytical solution of these rate equations to explore how the spatial pattern of activity of the hypercolumn depends on the parameters of the recurrent interactions (J_e, J_{in}, λ_e, and λ_{in}) and the stimulus properties.

5.1 Emergence of a Ring Attractor.
We first consider the case of an untuned LGN input, $\epsilon = 0$. In this case, equation 5.1 has a trivial solution in which all the neurons respond at the same firing rate. As shown in

appendix B, this solution is unstable when the spatial modulation of the effective interaction, equation 5.2, is sufficiently large. The condition for the onset of this instability is given by equation B.4. When the homogeneous solution is unstable, the system settles into a heterogeneous solution, which has the form $f(\theta) = M(\theta - \psi)$. The angle ψ is arbitrary and reflects the fact that the system is spatially invariant. The manifold of stable states that emerges in this system and breaks its spatial symmetry is known as a ring attractor. The function M, which represents the shape of the activity profile in each of these states, can be computed analytically, as described in appendix B. Depending on which mode is unstable, the heterogeneous profile of activity that emerges consists of a single "hill" of activity or several such "hills." In appendix B, we describe how the function M can be computed in the case of a state with a single hill.

As an example, we consider the case $\lambda_e = 11.5°$, $\lambda_{in} = 43°$, and $\beta J_{in} = 0.73$. For this choice of parameters, equation B.4 predicts that the state with a homogeneous response is stable for $\beta J_e < 0.87$ and unstable for $\beta J_e > 0.87$. At $\beta J_e = 0.87$, the unstable mode corresponds to the first Fourier mode. Therefore, the instability at this point should give rise to a heterogeneous response with a unimodal profile of activity (a single hill). This is confirmed by the numerical solution of the rate equations, 5.1 and 5.2.

Using the mapping prescriptions, equation 3.9, these results can be translated into the prediction that if $\lambda_e = 11.5°$, $\lambda_{in} = 43°$, $N_{in}\bar{G}_{in} = 0.333$ mS/cm^2, the homogeneous state is stable for conductance-based model if $N_e\bar{G}_e < 0.138$ mS/cm^2, but that it is unstable for $N_e\bar{G}_e > 0.138$ mS/cm^2. We tested whether these predictions coincide with the actual behavior of the conductance-based model in numerical simulations. Figures 4A and 4B show raster plots of the network for $N_e\bar{G}_e = 0.133$ mS/cm^2 and $N_e\bar{G}_e = 0.143$ mS/cm^2, respectively. For $N_e\bar{G}_e = 0.133$ mS/cm^2, neurons in all the columns responded in a similar way. This corresponds to the homogeneous state of the rate model. Moreover, in this simulation, the average population firing rate was $f = 18$ spikes/sec, in excellent agreement with the value predicted from the rate model for the corresponding parameters ($f = 18.05$ spikes/sec). In contrast, for $N_e\bar{G}_e = 0.143$ mS/cm^2, the network does not respond homogeneously to the stimulus. Instead, a unimodal hill of activity appears. This is congruent with the prediction of the rate model. Since the external input is homogeneous, the location of the peak is arbitrary. In the numerical simulations, the activity profile slowly moves due to the noise in the LGN input.

The stability analysis of the homogeneous state of the rate model shows that if $\beta J_{in} > 0.965$, which corresponds to $N_{in}\bar{G}_{in} = 0.443$ mS/cm^2, the mode $n = 2$ is the one that first becomes unstable when J_e increases. This suggests that in this case, the profile of activity that emerges through the instability is bimodal. Numerical simulations of the full conductance-based model were found to be in excellent agreement with this expectation (see Figure 5).
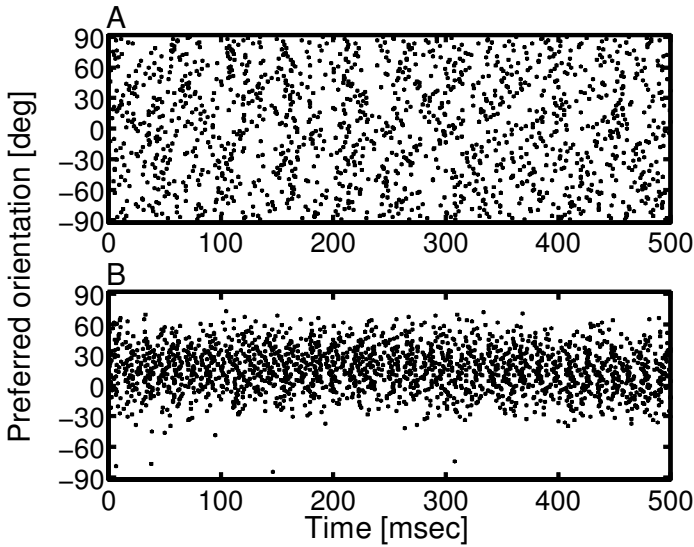
Figure 4: Symmetry breaking leading to a unimodal activity profile. A network with $N_e = N_{in} = 1600$ was simulated for two values of the maximal conductance of the excitatory synapses. The external input to the network is homogeneous ($\epsilon = 0$). The input rate is $\bar{f}_{LGN} = 2700\,\text{Hz}$. The maximal conductance of the input synapses is $G^{\text{inp}} = 0.0025\,\text{mS/cm}^2$. Parameters of the interactions are $\lambda_e = 11.5°$, $\lambda_{in} = 43°$, $N_{in}\bar{G}_{in} = 0.333\,\text{mS/cm}^2$. The time constants of the synapses are $\tau_e = \tau_{in} = 3\,\text{msec}$. The analytical solution of the rate model equations predicts that for $N_e\bar{G}_e < 0.138\,\text{mS/cm}^2$, the response of the network to the input is homogeneous and that for $N_e\bar{G}_e > 0.138\,\text{mS/cm}^2$, it is unimodal. (A) Raster plot of the network for $N_e\bar{G}_e = 0.133\,\text{mS/cm}^2$ showing that the response is homogeneous. (B) $N_e\bar{G}_e = 0.143\,\text{mS/cm}^2$, showing that the response is a unimodal hill of activity. The noise that is present in the system induces a slow random wandering of the hill of activity.

5.2 Tuning of Firing Rates and Synaptic Conductances. We consider now the case of a tuned LGN input, which corresponds to $\epsilon > 0$. Equation 5.1 shows that in general, the response of a neuron with PO θ depends on the stimulus orientation θ_0 through the difference $\theta - \theta_0$—namely, that $f(\theta, \theta_0) = M(|\theta - \theta_0|)$. For fixed θ_0, when θ varies, $f(\theta, \theta_0)$ is the profile of activity of the network in response to a stimulus of orientation θ_0. Conversely, when θ is fixed and θ_0 varies, $f(\theta, \theta_0)$ is the tuning curve of the neuron with PO θ. Therefore, the function M determines the tuning curve of the neurons in the model.

We now compare the tuning curves of the neurons computed in the framework of the rate model with those in the corresponding simulations
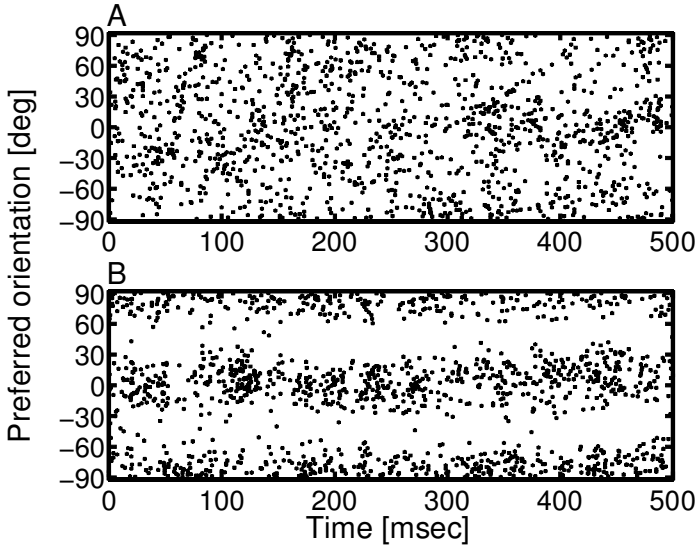
Figure 5: Symmetry breaking leading to a bimodal activity profile. The size of the simulated network is $N_e = N_{in} = 1600$. The input rate is $\bar{f}_{LGN} = 2700$ Hz. The maximal conductance of the input synapses is $G^{inp} = 0.0025$ mS/cm². The parameters of the interactions are $\lambda_e = 11.5°$, $\lambda_{in} = 43°$, $N_{in}G_{in} = 1.33$ mS/cm². The time constants of the synapses are $\tau_e = \tau_{in} = 3$ msec. The analytical solution of the rate model equations predicts that for $N_e\bar{G}_e < 0.196$ mS/cm², the response of the network to the input is homogeneous and that for $N_e\bar{G}_e > 0.196$ mS/cm², it is bimodal. (A) Raster plot of the network for $N_e\bar{G}_e = 0.19$ mS/cm², showing that the response is homogeneous. The average firing rate in the network in the simulation is $f = 3.2$ spikes/sec, which is in good agreement with the prediction of the rate model ($f = 2.9$ spikes/sec). (B) $N_e\bar{G}_e = 0.138$ mS/cm², showing that the response is bimodal. The noise that is present in the system induces a slow random wandering of the pattern of activity.

of the conductance-based network. Specifically, we take $\epsilon = 0.175$ and $\bar{f}_{LGN} = 3400$ Hz. For these values, in the absence of recurrent interactions, the response of the neurons to the input exhibits broad tuning. This is shown in Figure 6 (dashed line). The recurrent excitation can sharpen the tuning curves and also amplify the neuron response, as shown in Figure 6. In this figure, we plotted the neuronal tuning curve when the parameters of the interactions are $\lambda_e = 6.8°$ and $\lambda_{in} = 43°$, $N_e\bar{G}_e = 0.125$ mS/cm², $N_{in}\bar{G}_{in} = 0.333$ mS/cm². The solid line was computed from the solution of the mean-field equations of the corresponding rate model. This solution indicates that the tuning width is $\theta_C = 30°$ and that the maximal firing rate is $f_{max} = 75.5$ spikes/sec. The circles are from the numerical simulations of the
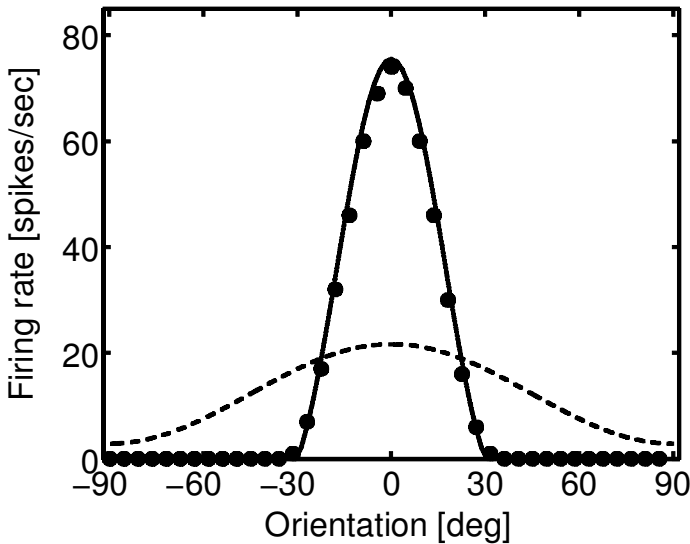
Figure 6: Tuning curves of the LGN input (dashed line) oriented at $\theta_0 = 0°$ and the spike response of a neuron with preferred orientation $\theta = 0°$ (solid line and circles). The LGN input parameters are $\epsilon = 0.175$, $g_{\text{inp}} = 0.0025$ mS/cm^2, $\bar{f}_{LGN} = 3400$ Hz. The interaction parameters are $\lambda_e = 6.3°$, $\lambda_{in} = 43°$, $N_e \bar{G}_e = 0.125$ mS/cm^2, $N_{in}\bar{G}_{in} = 0.467$ mS/cm^2. The time constants of the synapses are $\tau_e = \tau_{in} = 3$ msec. The circles are from numerical simulations with $N_e = N_{in} = 1600$ neurons. The response of the neuron was averaged over 1 sec of simulation. The solid line was obtained by solving the rate model with the corresponding parameters.

conductance-based model. The agreement with the analytical predictions from the rate model is very good.

The input conductances of the neurons in V1 change upon presentation of a visual stimulus. Experimental results (Borg-Graham, Monier, & Fregnac, 1998; Carandini, Anderson, & Ferster, 2000) indicate that with large stimulus contrasts, these changes have typical values of 60% when the stimulus is presented at null orientation, whereas they can be as large as 250 to 300% at optimal orientation. We applied our approach to study the dependence of the total change in input conductance on the space constants of the interactions for a given LGN input. We assume that the cortical circuitry sharpens and amplifies the response such that the tuning curves have a given width θ_C and amplitude $f_{\max}$. We compute the interaction parameters to achieve tuning curves with a given width, θ_C and a given maximal discharge rate, $f_{\max}$. To be specific, we take $\theta_C = 30.5°$, $f_{\max} = 70$ spikes/sec. We also fixed the space constant of the
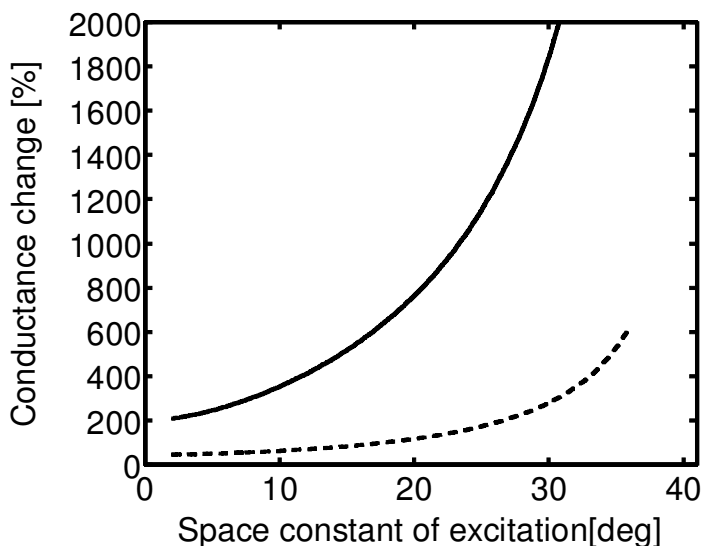
Figure 7: Change in the input conductance in iso (solid line) and cross-orientation (dashed line). The lines were computed as explained in the text.

inhibitory interaction, $\lambda_{in} = 43°$, and varied the value of λ_e. For each value of λ_e, we evaluated the values of J_e and J_{in} that yield the desired values of θ_C and f_{max}. Subsequently, for each set of parameters, we computed the changes in the input conductance of the neurons, relative to the leak conductance, for a stimulus presented in iso and cross orientation. These changes, denoted by Δg_{iso} and Δg_{cross}, respectively, are increasing functions of λ_e, as shown in Figure 7. Actually, it can be shown analytically from the mean field equations of the rate model that the conductance changes diverge when $\lambda_e \to \lambda_{in}$. This is because in that limit, the net interaction is purely excitatory with an amplitude that is above the symmetry-breaking instability.

The rate model also allows us to estimate the separate contributions of the LGN input, the recurrent excitation, and the cortical inhibition to the change in total input conductance induced by the LGN input. An example of the tuning curves of these contributions is shown in Figure 8, where they are compared with the results from the simulations of the full model. These results indicate that for the chosen parameters, most of the input conductance contributed by the recurrent interactions comes from the cortical inhibition. This is despite the fact that the spike discharge rate is greatly amplified by the cortical excitation.
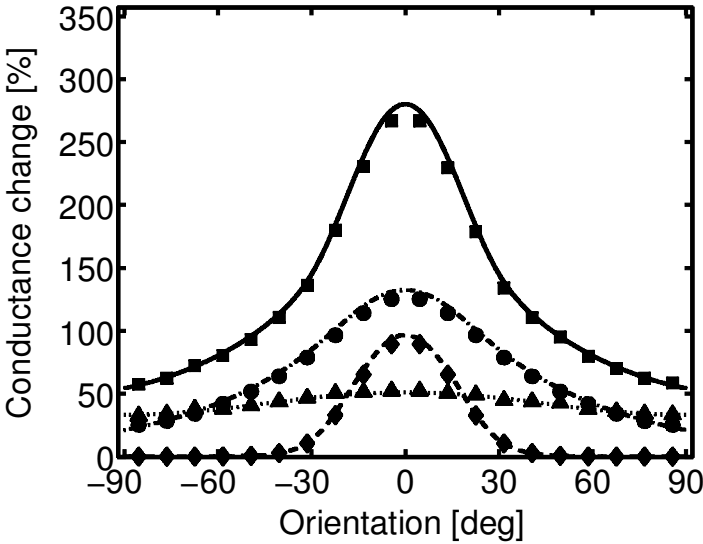
Figure 8: Tuning curves of conductances. Solid line: Total change. Dotted line: Contribution to the total change from the LGN input. Dashed line: Contribution to the total change from the recurrent excitatory interactions. Dash-dotted line: Contribution to the total change from the recurrent inhibitory interactions. These lines were obtained from the solution of the mean-field equations of the rate model. The parameters are as in Figure 6. The squares, circles, triangles, and diamonds are from numerical simulations. Same parameters as in Figure 6.

6 Rate Response of a Single Neuron to a Time-Dependent Input

The analysis of the previous sections focused on situations in which the firing rates of the neurons were approximately constant in time. We now turn to the question of firing-rate dynamics, namely, how to describe the neuronal firing response in the general situation in which the firing rates are time dependent.

We first study the response of a single neuron to a noisy sinusoidal input, equation 2.10. The firing rate of the neuron (averaged over the noise) can be expanded in a Fourier series:

$$f(t) = f_0 + f_1 \cos(\omega t + \phi) + \cdots, \tag{6.1}$$

where f_0 is the mean firing rate and f_1 and ϕ are the amplitude and phase of the first harmonic (the Fourier component at the stimulation frequency). Here, we consider only cases in which the modulation of the external input is not overly large, so that there is no rectification of the firing rate by the threshold.

Under these conditions, our simulations show that harmonics with orders higher than 1 are negligible (results not shown). Therefore, the response of the neuron can be characterized by the average firing rate f_0 and the modulation f_1, $f_1 < f_0$. Our simulations also show that the mean response, f_0, depends only weakly on the modulation frequency of the stimulus or on the stimulus amplitude and can be well described by the steady-state frequency-current relation. This is shown in Figure 9 (left panels), where the predictions from the rate model (solid horizontal lines) are compared with the mean output rates in the numerical simulations of the conductance-based model (open circles).

Figure 9 also shows the amplitude of the first harmonic of the response and its phase shift ϕ as a function of the modulation frequency $\nu \equiv \omega/2\pi$ (filled circles). It should be noted that the raw response of the neuron reflects two filtering processes of the external input rate: the low-pass filtering induced by the synaptic dynamics and the filtering induced by the intrinsic dynamics of the neuron and its spiking mechanism. To better elucidate the transfer properties of the neuron, we remove the effect of the synaptic low-pass filtering on the amplitude and phase of the response. (This corresponds to multiplying f_1 by $\sqrt{1 + \omega^2(\tau^{\text{inp}})^2}$ and subtracting $tan^{-1}(-\omega\tau^{\text{inp}})$ from the phase.) The results for two values of the mean output rate, $f_0 \simeq 30$ spikes/sec and $f_0 \simeq 60$ spikes/sec, and for two values of the input noise coefficient of variation, $\Delta = 0.18$ ($f_0^{\text{inp}} = 1125$ Hz) and $\Delta = 0.3$ ($f_0^{\text{inp}} = 3125$ Hz), are presented. Clearly, both the amplitude and the phase of the response depend on the modulation frequency. Of particular interest is the fact that the amplitude exhibits a resonant behavior for modulation frequencies close to the mean firing rate of the neuron, f_0. The main effect of increasing the coefficient of variation of the noise is to broaden the resonance peak.

As in our analysis of the steady-state properties, the external synaptic input can be decomposed here into a current term, and a conductance term, which are now time dependent. The simplest dynamic model would be to assume that the same f-I relation that was found under steady-state conditions, Equations 2.2 and 2.3, holds when the applied current and the passive conductance are time dependent. In our case, this would take the form $f(t) = \beta[I(t) - (I_c^o + V_c g(t))]_+$. This model predicts that the response amplitude does not depend on the modulation frequency and that the phase shift is always zero, in contrast to the behavior of the conductance-based neuron (see Figure 9). To account for the dependence of the modulation frequency, we extend the model by assuming that it has the form

$$f(t) = \beta[I_{\text{filt}}(t) - (I_c^o + V_c g_{\text{filt}}(t))], \tag{6.2}$$

where $I_{\text{filt}}(t)$ and $g_{\text{filt}}(t)$ are filtered versions of the current and conductance terms, respectively. For simplicity, we use the same filter for both current and conductance. A first-order linear filter can be either a high-pass or a low-pass
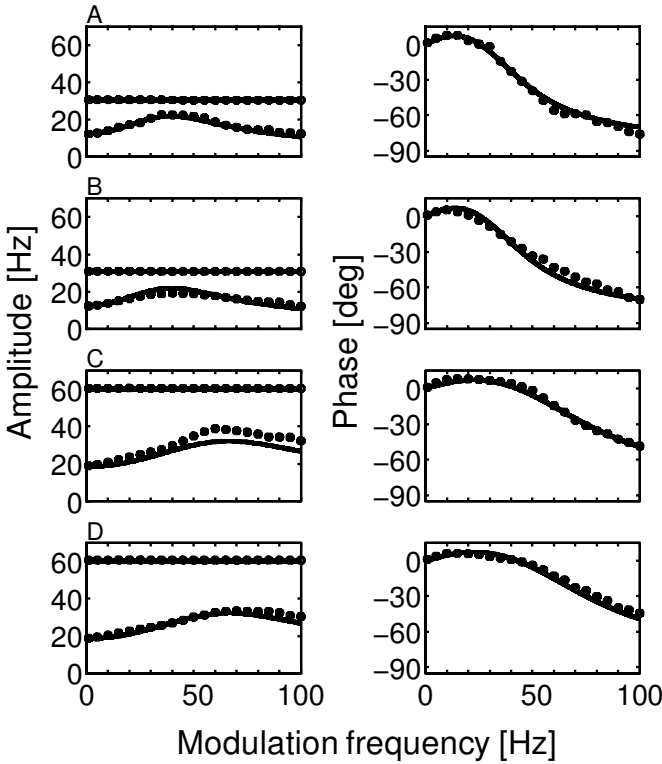
Figure 9: Mean, amplitude, and phase of single-neuron rate response as a function of the modulation frequency. The left panels show the mean output rate of the neuron (hollow circles) and the amplitude of the response (filled circles). The right panels show the phase of the response. The solid curves are the predictions of the dynamic rate model (see the text). The external input was designed to produce a mean output rate of about ~ 30 spikes/sec in A and B and ~ 60 spikes/sec in C and D. A and C show the responses to inputs with a small noise coefficient of variation, $\Delta = 1/\sqrt{2f_0^{\text{inp}} \tau^{\text{inp}}} = 0.18$, while B and D show the responses to inputs with a high noise level, $\Delta = 0.3$.

filter. Since the dependence of the response amplitude on the modulation frequency has a bandpass nature, a first-order linear filter would not be suitable. Thus, we assume a second-order linear filter. The filter for the current is described by

$$\frac{1}{\omega_0^2} \frac{d^2 I_{\text{filt}}}{dt^2} + \frac{1}{\omega_0 Q} \frac{dI_{\text{filt}}}{dt} + I_{\text{filt}} = I + \frac{a}{\omega_0} \frac{dI}{dt}, \tag{6.3}$$
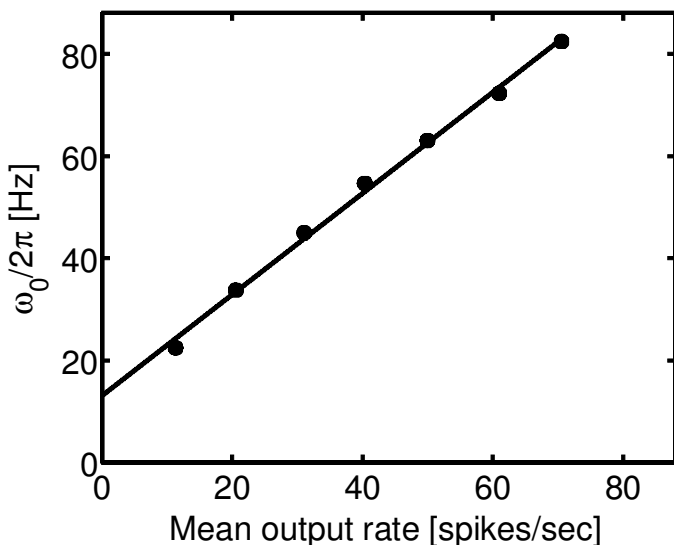
Figure 10: Resonance frequency ($\omega_0/2\pi$) as a function of the mean output rate. For each value of the mean output rate, optimal values of ω_0 were averaged over four noise levels: $\Delta = 0.15, 0.18, 0.22, 0.3$. The range of modulation frequencies for the fit was 1–100 Hz. The optimal linear fit (solid line) has a slope of 1 and an offset of 13.1.

and a similar equation (with the same parameters) defines the conductance filter. This is the equation of a damped harmonic oscillator with a resonance frequency $\omega_0/2\pi$ and Q-factor Q (Q is defined as ω_0 over the width at half height of the resonance curve). Note that the driving term is a linear combination of the driving current input and its derivative.

We investigated the behavior of the optimal filter parameters over a range of mean output rates, 10–70 spikes/sec, and a range of input noise levels, $\Delta = 0.15$–0.3. For lower noise levels, the response profile contains additional resonant peaks (both subharmonics and harmonics) that cannot be accounted for by the linear filter of equation 6.3. For each mean output rate and input noise level, we ran a set of simulations with modulation frequencies ranging from 1 Hz to 100 Hz, and then numerically found the set of filter parameters that gave the best fit for both amplitude and phase of the response. The variation of the optimal values for Q and a was small under the range of input parameters we considered, with mean values of $Q = 0.85$ and $a = 1.9$. The resonance frequency $\omega_0/2\pi$ depends only weakly on the noise level but increases linearly with the mean output rate of the neuron, with a slope of 1, $\omega_0/2\pi = f_0 + 13.1$, as shown in Figure 10. The solid curves in Figure 9 show the predictions of equation 6.3 for the amplitude and phase
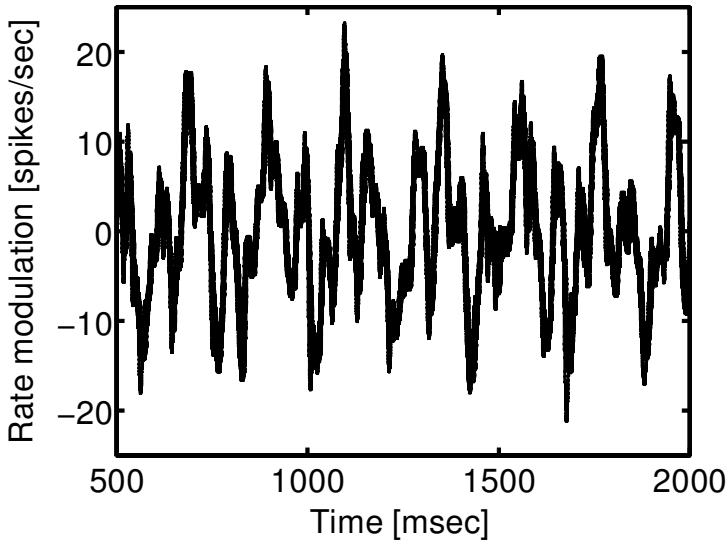
Figure 11: Single-neuron response to a broadband signal. The thick curve shows the rate of the conductance-based neuron, and the thin curve shows the prediction of the rate model. The input consisted of a superposition of 10 cosine functions with random frequencies, amplitudes, and phases (see text for specifics). For clarity, only the fluctuations around the mean firing rate ($\sim$ 30 spikes/sec) are shown.

of the rate response using the mean values of Q and a and the linear fit for ω_0, mentioned above. The results show that this model is a reasonable approximation of the response modulation of the conductance-based neuron.

So far, we have dealt with the firing-rate response of a single neuron to input composed of a single sinusoid. We also tested the response of the neuron to a general broadband stimulus. For this, we used a Poissonian input characterized by a mean rate and a time-varying envelope that consisted of a superposition of 10 cosine functions with random frequencies, amplitudes, and phases. The mean input rate was chosen to obtain a mean output firing rate $\sim$ 30 spikes/sec. The modulation frequencies were drawn from a uniform distribution between 0 and 60 Hz and the phases from a uniform distribution between 0 and 360°. The relative amplitudes were drawn from a uniform distribution between 0 and 1, and to avoid rectification, they were normalized so that their sum is 0.8. The results are presented in Figure 11. They show that the response to a broadband stimulus can be predicted from the response to each of the Fourier components. This confirms the validity of our linearity assumption, equation 6.2.

7 Response of a Neuronal Population to a Time Periodic Input ⎯⎯⎯

We now apply the approach of the previous section to study the dynamics of a network of interacting neurons in response to a time-dependent input. Here we consider the case of a large, homogeneous network of N fully connected neurons, which receive an external noisy oscillating input. The input to each neuron is a Poisson process with a sinusoidal envelope. In addition, the firing times of the inputs that converge on different cells in the network are uncorrelated, so that the Poissonian fluctuations in the inputs to the different cells are uncorrelated. Nevertheless, since the underlying oscillatory rate of the different inputs is coherent, the network response will have a synchronized component. To construct a simple model of the dynamics of the network rate, we first define two conductance-rate variables, $r(t) = g(t)/(NG\tau_e)$ and $r^{\mathrm{inp}}(t) = g^{\mathrm{inp}}(t)/(G^{\mathrm{inp}}\tau_e)$, where G and G^{inp} are the peak conductances of the recurrent and afferent synapses, respectively.

Averaging equation 2.7 over all the neurons in the network yields the following equation for the population conductance rate,

$$\tau_e \frac{dr}{dt} = -r + f(t), \tag{7.1}$$

where $f(t)$ is the instantaneous firing rate of the network per neuron. A similar equation holds for $r^{\mathrm{inp}}(t)$, which is a low-pass filter of $f^{\mathrm{inp}}(t)$. The equation for $f(t)$ is

$$f(t) = \beta[J^{\mathrm{inp}}\rho^{\mathrm{inp}} + J\rho - I_c], \tag{7.2}$$

where J^{inp} and J are given in equation 4.3. The quantities $\rho(t)$ and $\rho^{\mathrm{inp}}(t)$ are obtained from $r(t)$ and $r^{\mathrm{inp}}(t)$, respectively, using the filter in equation 6.3,

$$\frac{1}{\omega_0^2}\frac{d^2\rho}{dt^2} + \frac{1}{\omega_0 Q}\frac{d\rho}{dt} + \rho = r + \frac{a}{\omega_0}\frac{dr}{dt}, \tag{7.3}$$

and a similar equation holds for ρ^{inp}. This yields a set of self-consistent equations, which determine the firing rate of the neurons in the network, $f(t)$. For response modulation amplitudes smaller than the mean firing rate, the dynamics are linear and can be solved analytically (see appendix C). Figure 12 shows the mean, amplitude, and phase of the network response $f(t)$ obtained by simulating the dynamics of the conductance-based network together with the analytical predictions of the rate model. (As in the previous section, the filtering done by the input synapses was removed for purposes of presentation.) The mean rate of the Poisson input and the strength of the synaptic interaction were chosen such that the mean firing rate of the network will be around 50 spikes/sec and the noise level will be $\Delta = 0.22$.

The results of Figure 12 reveal the effect of the recurrent interactions on the modulation of the network rate response. Qualitatively, the peak of the
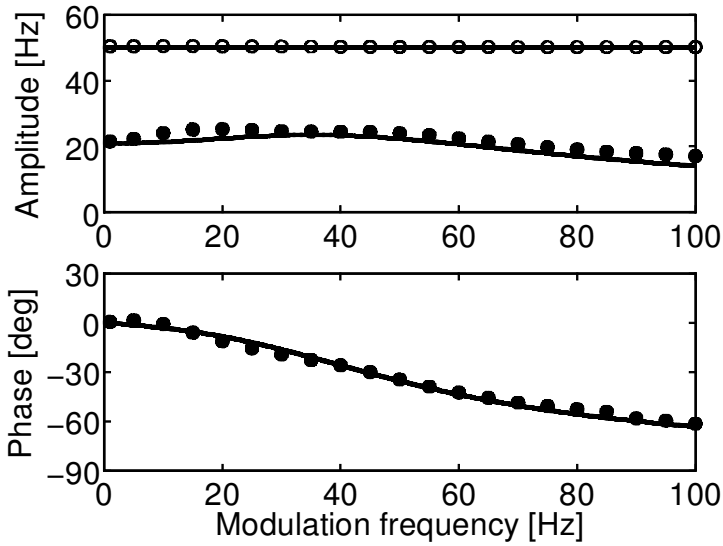
Figure 12: Response of an excitatory network to a sinusoidal stimulus. (Top) Mean (hollow circles) and amplitude (filled circles). (Bottom) Phase. The network consists of $N = 4000$ neurons. The neurons are coupled all-to-all. The synaptic conductance is $NG = 0.039$ mS/cm^2, and the synaptic time constant is $\tau_e = 5$ msec. The reversal potential of the synapses was $V_e = 0$ mV.

response amplitude profile is suppressed and shifts to smaller frequencies due to the excitatory connectivity. In contrast, for an inhibitory network, the model predicts that the peak response will be shifted to the right and that the resonant behavior will be more pronounced. This can be proved from equation C.2 by taking negative J. To test this prediction, we ran simulations of a uniform fully connected network with inhibitory synapses (the reversal potential was -80 mV). The input parameters and the strength of the synaptic interaction were chosen to produce a mean firing rate around 50 spikes/sec and a noise level $\Delta = 0.3$. Shown in Figure 13 are the results of the numerical simulations, together with the prediction of the rate model. These results provide additional strong support for our phenomenological time-dependent rate response model.

8 Discussion

The rate models derived here are based on specific assumptions about single cell properties. The most important assumptions are the independence of the gain of the f-I curve of the leak conductance, g_L (see equation 2.2) and the approximated linear dependence of the threshold current on g_L (see
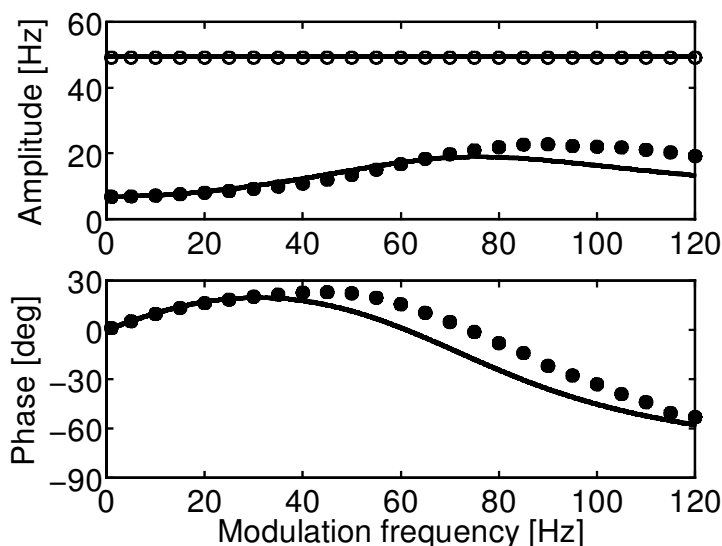
Figure 13: Response of an inhibitory network to a sinusoidal stimulus. (Top) Mean (hollow circles) and amplitude (filled circles). (Bottom) Phase. The network consists of $N = 4000$ neurons. The neurons are coupled all-to-all. The synaptic conductance is $NG = 0.18$ mS/cm^2, and the synaptic time constant is $\tau_e = 5$ msec. The reversal potential of the synapses was $V_{in} = -80$ mV.

equation 2.3). This means that shunting conductances have a subtractive effect rather than a divisive one. This is in agreement with previous modeling studies (Holt & Koch, 1997) and with the properties of the conductance-based model neuron used in our study (see Figure 2). Recent experiments using the dynamic clamp technique provide additional support for this assumption (Brizzi et al., 2001; Chance, Abbott, & Reyes, 2002). A further simplifying assumption, supported by experiments, is that in a broad range of input currents and output firing rates, the f-I curves of cortical neurons can be well approximated by a threshold linear function. We used such a form of the f-I curve to show that the response of a single neuron to a stationary synaptic input can be well described by simple rate models with threshold nonlinearity. We applied our single-neuron model to the study of a network of neurons, receiving an input generated by a set of synapses activated by uncorrelated trains of spikes with stationary Poisson statistics. In this case, we derived a rate model under the additional assumptions that the network is highly connected and that it is in an asynchronous state.

The mapping of the conductance-based model onto a rate model described in this work provides a correspondence between the "synaptic efficacy" used in rate models and biophysical parameters of the neurons. In

particular, the sign of the synaptic efficacy is determined by the value of the reversal potential relative to $E_L + V_c$, where V_c is the threshold gain-potential of the postsynaptic neuron (see equation 2.3). Furthermore, our theory enables the use of rate models to calculate synaptic conductances that are generated by the recurrent activity, allowing a quantitative comparison of predictions from rate models and conductance measurements in in vitro and in vivo intracellular experiments.

In the case of a fully connected network of excitatory neurons, we showed that the firing rate of the neurons predicted by the rate model was highly congruent with simulation results in a broad range of synaptic conductances. This indicates that our rate model provides reliable results over a broad range of firing rates and conductance changes. Even for very high rates, incorporating a weak quadratic nonlinearity is enough to account for the saturation of the neurons' firing rates. We also showed that our approach can be applied to networks with more complicated architectures, such as the conductance-based model of a hypercolumn in V1 analyzed in this work. The conditions for the stabilization of the homogeneous state can be correctly predicted from the mean-field analytical solution of the corresponding rate model. Furthermore, the profile of activity of the network and the tuning curve of the synaptic conductances can be calculated. Our results show that in order to obtain changes in input conductances that are similar to those found experimentally, one has to assume that the space constant of the excitatory feedback is much smaller than the space constant of the inhibitory interactions. However, this conclusion may depend on our assumption of interaction profiles, which are identical for excitatory and inhibitory targets.

To extend our approach to the case of time-dependent inputs, we studied the response of the single neuron to noisy input that is modulated sinusoidally in time. We showed that this response can be described by a rate model in which the neuron responds instantaneously to an effective input, which is a filtered version of the actual one. This is similar to the approach of Chance, du Lac, and Abbott (2001), who studied the responses of spiking neurons to oscillating input currents. Our description is valid provided that the input is sufficiently noisy to broaden resonances and that its modulation is small compared to its average to avoid rate rectification. Interestingly, if these assumptions are satisfied, we found that the neuron essentially behaves like a linear device even if the modulation of the input is substantial. This allowed us to derive a rate model that provides a good description for the dynamics of a homogeneous network of neurons receiving a time-dependent input.

Our derivation of rate equations for conductance-based models can be compared to the one suggested by Ermentrout (1994; see also Rinzel & Frankel, 1992). Ermentrout derived a rate model in the limit where the synaptic time constants are much longer than the time constants of the currents involved in the generation of spikes, as well as in the interspike

interval. In this case, the neuronal dynamics on the scale of the synaptic time constants can be reduced to rate equations of the type of equation 7.1 in which the rate variables, $r(t)$, represent the instantaneous activity of the slow synapses. However, in Ermentrout's approach, the firing rate $f(t)$ is given by an equation similar to equation 7.2 with $\rho^{inp} \equiv r^{inp}$ and $\rho \equiv r$. This is in contrast to our approach, where ρ^{inp} and ρ are filtered versions of r^{inp} and r. The two approaches become equivalent in the limit of slow varying input and slow synapses, that is, $\omega_0 \gg 1/t^{inp}$, $1/\tau_s$ where t^{inp} is the typical timescale over which the external input varies and τ_s is the synaptic time constant of the faster synapses in the network. The parameter ω_0 is the resonance frequency.

Knight (1972a, 1972b) studied the response of integrate-and-fire neurons to periodic input. He concluded that a resonant behavior occurred for input modulation frequencies around the average firing rate of the neurons. He also showed that white noise in the input broadens the resonance peak. Similar results were obtained by Gerstner (2000) in the framework of spike response models. This resonance has also been reported by Brunel, Chance, Fourcaud, and Abbott (2001) and Fourcaud and Brunel (2002), who studied analytically the firing response of a single integrate-and-fire neuron to a periodic input with temporally correlated noise. Our results extend these conclusions to conductance-based neurons. An interesting finding of this work is that the resonance frequency of the rate response increases linearly as a function of the mean output rate with a slope of one. It would be interesting to derive this relationship as well as the other parameters of our rate dynamics model from the underlying conductance-based dynamics. In addition, applications of our approach to other single-cell conductance-based models and to more complicated network architectures need to be explored. For instance, the effect of slow potassium adaptation currents should be taken into account. These currents are likely to contribute to the high-pass filtering of the neuron as shown by Carandini, Fernec, Leonard, and Movshon (1996) in the case of an oscillating injected current.

In this work, we used an A-current as a mechanism for the linearization of the f-I curve. Other slow hyperpolarizing conductances might also achieve the same effect (Ermentrout, 1998). In particular, slow potassium currents, which are responsible for spike adaptation in many cortical cells, might be alternative candidates. However, linear f-I curves are also observed in cortical inhibitory cells, most of which do not show spike adaptation, but they probably do possess an A-current.

Finally, we focused in this work on conductance-based network models of point neurons. An interesting open question is whether an appropriate rate model can also be derived for neurons with extended morphology. In conclusion, our results open up possibilities for applications of rate models to a range of problems in sensory and motor neuronal circuits in cortex as well as in other structures with similar single-neuron properties. Apply-ing the rate model to a concrete neuronal system requires knowledge of

a relatively small number of experimentally measurable parameters that characterize the f-I curves of the neurons in the system. In addition, the rate model requires knowledge of the gross features of the underlying connectivity pattern, as well as an estimate of the order of magnitude of the associated synaptic conductances.

Appendix A: Model Neuron

This appendix provides the specifics for the equations of the model neuron used here. The dynamics of our single-neuron model consists of the following equations

$$C_m \frac{dV}{dt} = -I_L - I_{Na} - I_K - I_A + I^{app}. \tag{A.1}$$

The leak current is given by $I_L = g_L(V - E_L)$. The sodium and the delayed rectifier currents are described in a standard way: $I_{Na} = \bar{g}_{Na} m_\infty^3 h(V - E_{Na})$ for the sodium current and $I_K = \bar{g}_K n^4 (V - E_K)$ for the delayed rectifier current. The gating variables $x = h, n$ satisfy the relaxation equations: $dx/dt = (x_\infty - x)/\tau_x$. The functions x_∞, ($x = h, n, m$), and τ_x are: $x_\infty = \alpha_x/(\alpha_x + \beta_x)$, and $\tau_x = \phi/(\alpha_x + \beta_x)$ where $\alpha_m = -0.1(V+30)/(\exp(-0.1(V+30)) - 1)$, $\beta_m = 4\exp(-(V + 55)/18)$, $\alpha_h = 0.07\exp(-(V - 44)/20)$, $\beta_h = 1/(\exp(-0.1(V+14))+1)$, $\alpha_n = -0.01(V+34)/(\exp(-0.1(V+34)) - 1)$ and $\beta_n = 0.125\exp(-(V + 44)/80)$. We have taken: $\phi = 0.1$.

The A-current is $I_A = \bar{g}_A a_\infty^3 b(V - E_K)$ with $a_\infty = 1/(\exp(-(V+50)/20) + 1)$. The function $b(t)$ satisfies $db/dt = (b_\infty - b)/\tau_A$ with: $b_\infty = 1/(\exp((V + 80)/6) + 1)$. For simplicity, the time constant, τ_A, is voltage independent.

The other parameters of the model are: $C_m = 1\mu F/cm^2$, $\bar{g}_{Na} = 100$ mS/cm^2, $\bar{g}_K = 40$ mS/cm^2. Unless specified otherwise, $g_L = 0.05$ mS/cm^2, $\bar{g}_A = 20$ mS/cm^2, and $\tau_A = 20$ msec. The reversal potentials of the ionic and synaptic currents are $E_{Na} = 55$ mV, $E_K = -80$ mV, $E_L = -65$ mV, $E_e = 0$ mV, and $E_{in} = -80$ mV. The external current is I_{app} (in $\mu A/cm^2$).

Appendix B: Model of a Hypercolumn in V_1: The Mean-Field Equations

B.1 The Instability of the Homogeneous State. For a homogeneous input, a trivial solution to the fixed-point equation, equation 5.1, corresponds to a state in which the responses of all the neurons are the same. However, this homogeneous state can be unstable if the spatial modulation of the interactions is sufficiently large. The condition for this instability can be derived by solving equation 5.1 in the limit of a weakly heterogeneous input $f_{LGN}(\theta)$ as follows.

The Fourier expansion of f_{LGN} is

$$f_{LGN}(\theta) = \sum_{n=1}^{\infty} f_n \exp(2in\theta), \tag{B.1}$$

where the coefficients f_n are complex numbers. For weakly heterogeneous inputs, all the coefficients but f_0 are small. In the parameter regime where the homogeneous state is stable, the response of the network to this input will be weakly heterogeneous. Therefore, the Fourier expansion of the activity profile is,

$$m(\theta) = \sum_{n=1}^{\infty} m_n \exp(2in\theta), \tag{B.2}$$

where all the coefficients but m_0 are small. Substituting equations B.1 and B.2 in equation 5.1 and computing the coefficients $m_n, n > 0$ perturbatively, one finds:

$$m_n = \frac{J_{LGN} f_n}{1 - \beta J_n}, \tag{B.3}$$

where J_n are the Fourier coefficients of the interactions.

The coefficient m_n diverges if $\beta J_n = 1$. This divergence indicates an instability of the homogeneous state. This instability induces a heterogeneous profile of activity with n peaks.

The coefficients J_n can be computed from equation 5.2. This yields the instability onset condition:

$$2\beta \left(J_e \frac{1-(-1)^n \exp(-\pi/2\lambda_e)}{1+4n^2\lambda_e^2} + J_{in} \frac{1-(-1)^n \exp(-\pi/2\lambda_{in})}{1+4n^2\lambda_{in}^2} \right) = 1. \tag{B.4}$$

B.2 Mean-Field Equations for Profile of Activity. We are interested in the case in which the LGN input is broadly tuned, $0 < \epsilon < 1/2$, and the effect of the interactions is sufficiently strong to sharpen substantially the response of the neurons. More specifically, we require that $f(\theta) = 0$ for all the neurons with POs such that $|\theta - \theta_0| > \pi/2$. In this case, the solution to equations 5.1 and 5.2 can be found analytically. Taking $\theta_0 = 0$, without loss of generality, this solution has the form

$$f(\theta) = A_0 + A_1 \cos(\mu_1\theta) + A_2 \sin(\mu_2\theta) + A_3 \cos(2\theta) \quad \text{for } |\theta| < \theta_c \tag{B.5}$$

$$f(t) = 0 \qquad \text{for } \theta_c < |\theta| \tag{B.6}$$

The angle θ_c is determined by

$$f(\pm\theta_c) = 0. \tag{B.7}$$

Substituting equation B.5 in equation 5.1, one finds that μ_1 and μ_2 are solutions (real or imaginary) of the equation

$$\sum_{\alpha=E,I} \frac{2J_\alpha}{1 + \lambda_\alpha^2 x^2} = 1, \tag{B.8}$$

and that the coefficients A_0 and A_3 are given by

$$A_0 = \frac{\bar{J}_{LGN} f_{LGN}(1 - \epsilon) - T}{1 - 2J_e - 2J_{in}} \tag{B.9}$$

$$A_3 = \frac{\bar{J}_{LGN} f_{LGN}}{1 - 2\left(\frac{\mu_1 J_e}{1+4\mu_1^2} + \frac{\mu_2 J_{in}}{1+4\mu_2^2}\right)}. \tag{B.10}$$

Finally, A_1 and A_2 are obtained from the two equations:

$$F(\lambda_\alpha, \mu, \mathbf{A}) = 0 \qquad \alpha = E, I, \tag{B.11}$$

where, $\mu = (\mu_1, \mu_2)$, $\mathbf{A} = (A_0, A_1, A_2, A_3)$ and F is the function

$$F(x, \mu, \mathbf{A}) = A_0 + \sum_{i=1,3} \frac{A_i}{1 + \mu_i x^2}(\cos(\mu_i\theta_c) - \mu_i x \sin(\mu_i\theta_c)) \tag{B.12}$$

with $\mu_3 = 2$ and the angle θ_c is determined by the condition

$$A_0 + A_1 \cos(\mu_1\theta_c) + A_2 \sin(\mu_2\theta_c) + A_3 \cos(2\theta_c) = 0. \tag{B.13}$$

Appendix C: Rate Dynamics in a Neuronal Population with Uniform Connectivity

By Fourier transforming equations 7.1, 7.2, and 6.3 (assuming that the firing rates are always positive), we obtain for $\omega \neq 0$,

$$\hat{f}(\omega) = \beta(J^{inp}\hat{\rho}^{inp} + J\hat{\rho}), \tag{C.1}$$

where $\hat{\rho}(\omega) = B(\omega)\hat{r}(\omega)$, $\hat{r}(\omega) = L(\omega)\hat{f}(\omega)$, $\hat{\rho}^{inp}(\omega) = B(\omega)\hat{r}^{inp}(\omega)$, $\hat{r}^{inp}(\omega) = L(\omega)\hat{f}^{inp}(\omega)$. The low-pass filter $L(\omega)$ and bandpass filter $B(\omega)$ are given by $L(\omega) = 1/1 + i\omega\tau_e$ and $B(\omega) = (1 + ia\omega/\omega_0)/(1 + iw/\omega_0 - \omega^2/\omega_0^2)$.

Putting the above relations in equation C.1 and solving for $\hat{f}(\omega)$ gives the transfer function of the network,

$$\hat{f}(\omega) = \frac{\beta J^{inp} B(\omega)L(\omega)}{1 - \beta J B(\omega)L(\omega)} \hat{f}^{inp}(\omega), \tag{C.2}$$

which can be used to predict the time-dependent rate response.

References

Abbott, L. F., & Kepler, T. (1990). Model neurons: From Hodgkin-Huxley to Hopfield. In L. Garrido (Ed.), *Statistical mechanics of neural networks* (pp. 5–18). Berlin: Springer-Verlag.

Ahmed, B., Anderson, J. C., Douglas, R. J., Martin, K. A., & Whitteridge, D. (1998). Estimates of the net excitatory currents evoked by visual stimulation of identified neurons in cat visual cortex. *Cereb. Cortex, 8*, 462–476.

Amit, D. J. (1989). *Modeling brain function*. Cambridge: Cambridge University Press.

Amit, D. J., & Tsodyks, M. V. (1991). Quantitative study of attractor neural networks retrieving at low spike rates I: Substrate—spikes, rates and neuronal gain. *Network, 2*, 259–273.

Azouz, R., Gray, C. M., Nowak, L. G., & McCormick, D. A. (1997). Physiological properties of inhibitory interneurons in cat striate cortex. *Cereb. Cortex, 7*, 534–545.

Ben-Yishai, R., Lev Bar-Or, R., & Sompolinsky, H. (1995). Theory of orientation tuning in visual cortex. *Proc. Natl. Acad. Sci. USA, 92*, 3844–3848.

Borg-Graham, L. J., Monier, C., & Fregnac, Y. (1998). Visual input evokes transient and strong shunting inhibition in visual cortical neurons. *Nature, 393*, 369–373.

Brizzi, L., Hansel, D., Meunier, C., van Vreeswijk, C., & Zytnicki, D. (2001). Shunting inhibition: A study using in vivo dynamic clamp on cat spinal motoneurons. *Society for Neuroscience Abstract, 934.3*.

Brunel, N., Chance, F. S., Fourcaud, N., & Abbott, L. F. (2001). Effects of synaptic noise and filtering on the frequency response of spiking neurons. *Phys. Rev. Lett., 86*, 2186–2189.

Carandini, M., Fernec, M., Leonard, C. S., & Movshon, J. A. (1996). Spike train encoding by regular-spiking cells of the visual cortex. *J. Neurophysiol., 76*, 3425–3441.

Carandini, M., Anderson, J., & Ferster, D. (2000). Orientation tuning of input conductance, excitation, and inhibition in cat primary visual cortex. *J. Neurophysiol., 84*, 909–926.

Chance, F. S., du Lac, S., & Abbott, L. F. (2001). An integrate-or-fire model of spike rate dynamics. *Society for Neuroscience Abstract, 821.44*.

Chance, F. S., Abbott, L. F., & Reyes, A. D. (2002). Gain modulation from background synaptic input. *Neuron, 35*, 773–782.

Churchland, P. S., & Sejnowski, T. J. (1992). *The computational brain*. Cambridge, MA: MIT Press.

Connors, B. W., Malenka, R. C., & Silva, L. R. (1988). Two inhibitory postsynaptic potentials, and GABA$_A$ and GABA$_B$ receptor-mediated responses in neocortex of rat and cat. *J. Physiol. (Lond.), 406*, 443–468.

Ermentrout, B. (1994). Reduction of conductance based models with slow synapses to neural nets. *Neural Comp., 6*, 679–695.

Ermentrout, B. (1998). Linearization of F-I curves by adaptation. *Neural Comp., 10*, 1721–1729.

Fourcaud, N., & Brunel, B. (2002). Dynamics of the firing probability of noisy integrate-and-fire neurons. *Neural Comp., 14*, 2057–2111.

Georgopoulos, A. P., & Lukashin, A. V. (1993). A dynamical neural network model for motor cortical activity during movement: Population coding of movement trajectories. *Biol. Cybern., 69*, 517–524.

Gerstner, W. (2000). Population dynamics of spiking neurons: Fast transients, asynchronous states, and locking. *Neural Comp., 12*, 43–89.

Ginzburg, I., & Sompolinsky, H. (1994). Theory of correlations in stochastic neuronal networks. *Phys. Rev. E, 50*, 3171–3191.

Hansel, D., & Sompolinsky, H. (1996). Chaos and synchrony in a model of a hypercolumn in visual cortex. *J. Comput. Neurosci., 3*, 7–34.

Hansel, D., & Sompolinsky, H. (1998). Modeling feature selectivity in local cortical circuits. In C. Koch & I. Segev (Eds.), *Methods in neuronal modeling: From synapses to networks* (2nd ed., pp. 499–567). Cambridge, MA: MIT Press.

Hille, B. (1984). *Ionic channels of excitable membranes*. Sunderland, MA: Sinauer.

Hodgkin, A. L., & Huxley, A. F. (1952). A quantitative description of membrane current and its application to conduction and excitation in nerve. *J. Physiol. (Lond.), 117*, 500–562.

Holt, G. R., & Koch, C. (1997). Shunting inhibition does not have a divisive effect on firing rates. *Neural Comput., 9*, 1001–1013.

Hopfield, J. J. (1984). Neurons with graded response have collective computational properties like those of two-state neurons. *Proc. Natl. Acad. Sci. USA, 79*, 1554–2558.

Kernell, D. (1968). The repetitive impulse discharge of a simple model compared to that of spinal motoneurones. *Brain Research, 11*, 685–687.

Knight, B. W. (1972a). Dynamics of encoding in a population of neurons. *J. Gen. Physiol., 59*, 734–766.

Knight, B. W. (1972b). The relationship between the firing rate of a single neuron and the level of activity in a population of neurons. Experimental evidence for resonant enhancement in the population response. *J. Gen. Physiol., 59*, 767–778.

Press, W. H., Flannery, B. P., Teukolsky, S. A., & Vetterling, W. T. (1988). *Numerical recipes in C: The art of scientific computing*. Cambridge: Cambridge University Press.

Rinzel, J., & Frankel, P. (1992). Activity patterns of a slow synapse network predicted by explicitly averaging spike dynamics. *Neural Comp., 4*, 534–545.

Rolls, E. T., & Treves, A. (1998). *Neural networks and brain function*. New York: Oxford University Press.

Salinas, E., & Abbott, L. F. (1996). A model of multiplicative neural responses in parietal cortex. *Proc. Natl. Acad. Sci. USA, 93*, 11956–11961.

Seung, H. S. (1996). How the brain keeps the eyes still. *Proc. Natl. Acad. Sci. USA, 93*, 3339–13344.

Stafstrom, C. E., Schwindt, P. C., & Crill, W. E. (1984). Repetitive firing in layer V neurons from cat neocortex in vitro. *J. Neurophysiol., 52*, 264–277.

Wilson, H. R., & Cowan, J. (1972). Excitatory and inhibitory interactions in localized populations of model neurons. *Biophys. J., 12*, 1–24.

Zhang, K. (1996). Representation of spatial orientation by the intrinsic dynamics of the head-direction cell ensemble: A theory. *J. Neurosci., 16*, 2112–2126.